Wetting of rings on a nanopatterned surface: A lattice model study

Fabien Porcheron and Peter A. Monson*
Department of Chemical Engineering, University of Massachusetts, 159 Goessmann Laboratory, 686 North Pleasant Street, Amherst, Massachusetts 01003-9303, USA

Martin Schoen
Stranski-Laboratorium für Physikalische und Theoretische Chemie, Technische Universität Berlin, Strasse des 17, Juni 124, D-10623 Berlin, Germany
(Received 14 October 2005; published 10 April 2006)

We perform mean-field density functional theory calculations on a lattice model to study the wetting of a solid substrate decorated with a ring pattern of nanoscale dimensions. We have found three different liquid morphologies on the substrate: a ring morphology where the liquid covers the pattern, a bulge morphology where a droplet is forming on one side of the ring, and a morphology where the liquid forms a cap spanning the nonwetting disk inside the pattern. We investigate the relative stability of these morphologies as a function of the ring size, wall-fluid interaction, and temperature. The results found are in very good agreement with experiments and calculations performed on similar systems at a micrometer length scale. The bulge morphology has also been observed in Monte Carlo simulations of the lattice model. Our results show that (i) morphologies of wetting patterns previously observed on a much larger (μm) scale can also form on a nm length scale, (ii) whether or not this happens depends crucially on the size of the wettable pattern, and (iii) the wettable ring may only be partially wet by the bulge morphology of the fluid. This morphology is a result of a spontaneously broken symmetry in the system.

DOI: 10.1103/PhysRevE.73.041603 PACS number(s): 68.08.Bc, 61.46.−w, 62.25.+g, 68.35.Md

I. INTRODUCTION

The wetting of solid surfaces by liquids is a phenomenon which has attracted a great deal of attention for many years [1–3]. A droplet forms on a surface when it is thermodynamically more favorable for the fluid to partially condense rather than remain as a homogeneous vapor [1]. This situation happens when the system is in a supersaturated state—i.e., when the chemical potential μ is greater than its value at bulk gas-liquid coexistence μ_0. In this regime, the stable state is the bulk liquid but the low density of fluid available precludes a transition to this state. If the surface is ideal (i.e., with no defects of any kind), then the contact angle θ formed by a macroscopic droplet with this surface is described by Young's equation [4]

$$\sigma_{sl} - \sigma_{sv} + \sigma_{lv} \cos\theta = 0, \tag{1.1}$$

where σ_{sv}, σ_{sl}, and σ_{lv} are the solid-vapor, solid-liquid, and liquid-vapor surface tensions, respectively. The droplet is seen here as a spherical cap-shaped aggregate of the liquid phase surrounded by the metastable vapor.

Young's equation is macroscopic in nature and is not universally applicable. For instance, Eq. (1.1) only takes into account the change in free energy generated by the creation of an interfacial area between two phases, therefore neglecting the contact line formed at the interface of the solid-liquid-vapor phases. This contribution becomes important at small droplet sizes and a more general form of Young's equation known as the Gretz equation [5] gives

$$\sigma_{sl} - \sigma_{sv} + \sigma_{lv} \cos\theta + \frac{\tau_{slv}}{R \sin\theta} = 0, \tag{1.2}$$

where τ_{slv} is the line tension and R is the droplet radius.

A real surface also displays heterogeneities which can alter the contact angle of the droplet. The perturbation can either be energetic where a specific location of the surface interacts differently with the fluid or geometric where the surface is not smooth and aggregates of solid are present over the surface plane. The Cassie-Baxter and Wenzel equations represent generalization to heterogeneous surfaces of Young's equation for homogeneous surfaces. The Cassie-Baxter equation [6,7] is given by

$$\cos\theta_{app} = f_1 \cos\theta_1 + f_2 \cos\theta_2, \tag{1.3}$$

where θ_{app} is the apparent contact angle on the surface. In this approach the surface is viewed as made up of two types of patches 1 and 2 and the cosine of the apparent contact angle is a linear combination of the cosines of the contact angles (θ_1 and θ_2) on those homogeneous surfaces with each weighted by the surface area fraction. The Wenzel equation [8] gives

$$\cos\theta_{app} = r \cos\theta, \tag{1.4}$$

where θ is the contact angle on the homogeneous surface and r is the ratio of the actual area of liquid-solid contact to the projected area on the horizontal plane. It should be emphasized that Eqs. (1.1)–(1.4) apply to the formation of macroscopic droplets where, for example, the notion of a contact angle makes sense in that one can actually see the surface of the droplet and determine the angle at which it makes contact with the plane of the solid substrate. At molecular length

*Electronic address: monson@ecs.umass.edu

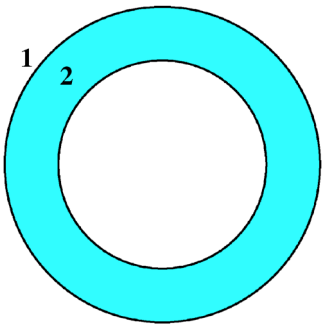

FIG. 1. (Color online) Geometry of the ring pattern. Surface **1** is nonwetting and surface **2** has a preferential attraction for the liquid.

scales contact angles need a more careful definition because of the diffuseness of the interfaces at these scales.

Over the last decade, researchers have made substantial progress in controlling surface heterogeneities even down to the nanometer length scale. It is now possible to imprint specific geometric or energetic patterns on a surface at such a small length scale [9–17]. At the length scales pertaining to individual molecules or small molecular assemblies the contact angle is an ill-defined quantity and macroscopic theoretical treatments are reasonably subject to question. For this reason the wetting properties of surfaces endowed with nanoscopic heterogeneities have received significant attention from theory and molecular simulations, which are well suited to study these kinds of systems. For instance, a surface can be decorated with stripes of variable dimensions which show a preferential attraction for the liquid. This gives rise to the emergence of new properties and phases which have been studied using both theory and simulations [18–40].

Another example is the imprinting of ring patterns over the surface [14]. In this situation, the pattern is characterized by an inner radius R_{in} and an outer radius R_{out} forming an annulus of constant width in which the surface displays a preferential interaction for the fluid (see Fig. 1). Those surfaces may be prepared by microcontact printing using alkanethiols on gold [13,14]. In this method an elastomer stamp is used to deposit molecules on surfaces. The stamp is first "inked" with a solution of alkanethiol molecules and then pressed onto a gold surface, which results in well-defined hydrophilic sites. Then the remaining bare gold surface is made hydrophobic by a dipping into another alkanethiol. A liquid is then subsequently adsorbed onto the surface in a closed cell. The experiments are conducted by cooling down or heating up the system, thereby changing the volume of liquid formed on the surface [14]. Experiments performed on these ring-patterned substrates show that when the volume increases, the liquid geometry formed over the pattern undergoes a transition from a ring morphology (where the liquid forms a homogeneous covering over the pattern) to a bulge morphology where a droplet of liquid is formed over one side of the pattern. This bulge geometry "breaks" the symmetry imposed by the pattern. As the volume of liquid increases, the bulge progressively spreads over the nonwetting disk inside the pattern and finally a spherical cap is formed over the whole disk of radius R_{out}. This bulge geometry can also be observed on surfaces patterned with micrometric stripes [29].

Lenz *et al.* [36] have modeled the wetting of surface imprinted with rings of micrometric dimensions. In their calculations, the macroscopic total interfacial free energy of the system is numerically minimized under a condition of constant liquid volume V [29–33,36]. Their numerical results describe correctly the experimental results as a morphological transition from a ring to a bulge geometry is observed when the volume of liquid increases. It is interesting to ask whether this phenomenology persists down to nanometer length scales. To investigate this question a molecular-based model is necessary since the continuum assumptions implicit in the approach of Lenz *et al.* [36] may fail at small length scales.

In this paper, we investigate the formation of liquid morphologies over surfaces imprinted with ring patterns of nanometric dimensions. We perform a set of calculations using a mean-field density functional theory (MF-DFT) on a lattice model. The lattice model provides a useful compromise that allows us to study systems between microscopic and mesoscopic sizes while maintaining computational tractability. This model has had significant success in the modeling of fluid confinement into mesoporous materials (e.g., in gas adsorption or liquid porosimetry) [41–47]. In the present application the grand canonical ensemble used in these works is not suitable because liquid droplets correspond to supersaturated (metastable) states of the bulk vapor, an effect of the curvature of the vapor-liquid interface [48] that becomes very large for nanoscale droplets. A similar situation arises in studies of free droplets in finite volumes [49,50]. Calculations in the grand canonical ensemble allow variations of the total density, and the morphological transitions of interest in our system are preempted by the bulk vapor-liquid phase transition. Therefore we implement an algorithm that allows us to solve the mean-field equations in the canonical ensemble (N-V-T) where the mean density of the system is fixed [47,51,52] and we can access supersaturated states of the bulk vapor. The experiments conducted on these systems [14] are carried out on a length scale of the order of a μm, and the curvature effect on the vapor-liquid interface and the degree of supersaturation in the vapor phase is quite small. We refer the reader to a recent article by Lipowsky [32] for additional discussion of the interpretation of experiments on the wetting of chemically structured surfaces. Both the experiments [14] and our calculations correspond to the third scenario described in Sec. 3.1 of that article.

The remainder of this paper is organized as follows. In Sec. II we present the models and methods relative to our calculations. The results are described in Sec. III, and conclusions from this work are presented in Sec. IV.

II. MODELS AND METHODS

A. Lattice Hamiltonian

To study the wetting of nanopatterned substrates we discretize the space by employing a lattice model. In our model spherically symmetric fluid molecules are restricted to sites on a simple cubic lattice such that each molecule has six nearest neighbors. Each site can be occupied by a single

molecule at most or it can be empty. The former condition accounts for a short-ranged repulsion between a pair of molecules. Hence, a configuration of the lattice fluid may be represented by the $\mathcal{N}$-dimensional vector $\mathbb{N}=(n_1,n_2,\ldots,n_{\mathcal{N}})$, where $\mathcal{N}$ is the total number of sites on the lattice and

$$n_i=\begin{cases}0, & \text{lattice site empty},\\ 1, & \text{lattice site occupied},\end{cases} \qquad i=1,\ldots,\mathcal{N}, \quad (2.1)$$

is the occupation number at site i. The characteristic energy function (i.e., the Hamiltonian) of our lattice fluid may then be cast as

$$H(\mathbb{N})=-\frac{\epsilon}{2}\sum_{i=1}^{\mathcal{N}}\sum_{j\neq i}^{\mathrm{NN}(i)} n_i n_j+\sum_{i=1}^{\mathcal{N}} n_i\Phi_i^{\mathrm{wf}}, \quad (2.2)$$

where $\epsilon>0$ determines the strength of attraction between a pair of fluid molecules and

$$\Phi_i^{\mathrm{wf}}=\sum_k v_{ik}^{\mathrm{wf}}(r_{ik}) \quad (2.3)$$

is the total energy between a fluid molecule at site i and the solid substrate. Hence, the sum on k in the previous equation extends over lattice sites pertaining to the solid substrate. The sum on j in Eq. (2.2) extends over the nearest-neighbor sites NN (i) of site i. Thus, we model fluid-fluid attraction according to a (short-range) square-well potential where we assume the width of the attractive well to be identical to the lattice constant.

In this work the solid substrate is decorated with wettable rings of inner radius R_{in} and outer radius R_{out}. We label a ring pattern using the notation $R_{\mathrm{in}}-R_{\mathrm{out}}$ so that a ring with an inner radius of 15 sites and an outer radius of 20 sites will be denoted as a 15-20 ring. We model v_{ik}^{wf} using a Lennard-Jones 12-6 potential

$$v_{ik}^{\mathrm{wf}}(r_{ik})=\begin{cases}4\alpha\epsilon(r_{ik}^{-12}-r_{ik}^{-6}), & k\in \text{ring},\\ 0, & k\notin \text{ring}.\end{cases} \quad (2.4)$$

Here α is the ratio of the fluid-solid Lennard-Jones well depth to the nearest-neighbor fluid-fluid interaction strength. In our calculations we shift the z coordinates so that the interaction energy for a fluid site adjacent to the ring surface and its nearest-neighbor surface site is $-\alpha\epsilon$. We have used two values of α ($\alpha=0.2$ and $\alpha=0.3$) to investigate the effect of this parameter on the wetting properties. For both these values of a uniform surface would be completely wetted (the contact angle is zero) by the fluid. For the case of $\alpha=0$ the surface is completely nonwetting (the contact angle is 180°). We can refer to the ring surfaces as being hydrophilic or lyophilic and the remainder of the surface as hydrophobic or lyophobic.

B. Mean-field density functional theory

Let us assume our lattice fluid to be coupled to an infinitely larger reservoir of matter. Its equilibrium states are then given by minima of the grand potential

$$-\beta\Omega(T,\mu)=\ln\Xi(T,\mu)=\ln\sum_{\mathbb{N}}\exp\left\{-\beta\left[H(\mathbb{N})-\mu\sum_{i=1}^{\mathcal{N}}n_i\right]\right\}, \quad (2.5)$$

where $\beta\equiv 1/k_{\mathrm{B}}T$ (k_{B} Boltzmann's constant), T denotes the temperature, μ is the chemical potential, and Ξ is the grand canonical partition function in standard notation. Let us also assume that we may write

$$H(\mathbb{N};\lambda)=H_0(\mathbb{N})+\lambda H_1(\mathbb{N}), \quad (2.6)$$

where H_0 and H_1 are the Hamiltonians governing some reference system (subscript 0) and a perturbation (subscript 1), respectively, and $0\leqslant\lambda\leqslant 1$ is a dimensionless parameter that serves to switch continuously between the reference system ($\lambda=0$) and the system of interest ($\lambda=1$). Inserting Eq. (2.6) into the far right side of Eq. (2.5) and introducing a mean-field approximation in terms of a set of undetermined parameters $\{\Psi_i\}$, namely,

$$H_0(\mathbb{N})\equiv\sum_{i=1}^{\mathcal{N}}\Psi_i n_i, \quad (2.7)$$

we eventually arrive at the Euler-Lagrange equation

$$\beta^{-1}\ln\frac{\rho_i}{1-\rho_i}-\epsilon\sum_{j\neq i}^{\mathrm{NN}(i)}\rho_j+\Phi_i^{\mathrm{wf}}-\mu=0, \quad i=1,\ldots,\mathcal{N}, \quad (2.8)$$

through a variational calculation. Equation (2.8) forms the basis of the calculations presented below. Details of this derivation can be found in Ref. [53].

The treatment so far implicitly assumes that the fluid in contact with the solid surface is coupled to an infinitely large bulk reservoir of matter. However, as discussed in the Introduction we want to solve the equations for a fixed overall density in the system, so we are interested in minima of the Helmholtz free energy defined through the Legendre transform

$$F\equiv\Omega+\mathcal{N}\bar{\rho}\mu, \quad (2.9)$$

where the mean density $\bar{\rho}$ is given by

$$\bar{\rho}\equiv\frac{1}{\mathcal{N}}\sum_{i=1}^{\mathcal{N}}\rho_i. \quad (2.10)$$

Equilibrium states correspond to minima of F subject to the constraint

$$\sum_{i=1}^{\mathcal{N}}\rho_i-\mathcal{N}\bar{\rho}=0; \quad (2.11)$$

that is, we are seeking solutions of the equation

$$\frac{\partial}{\partial \rho_i}\left[F-\eta\left(\sum_{i=1}^{\mathcal{N}}\rho_i-\mathcal{N}\bar{\rho}\right)\right]$$

$$=\beta^{-1}\ln\frac{\rho_i}{1-\rho_i}-\epsilon\sum_{j\neq i}^{\mathrm{NN}(i)}\rho_j+\Phi_i^{\mathrm{wf}}-\eta=0,\quad i=1,\ldots,\mathcal{N}, \tag{2.12}$$

where η is an as-yet-undetermined Lagrangian multiplier. However, comparison of Eqs. (2.8) and (2.12) leads us to conclude that $\eta=\mu$ if both approaches are required to give the same equilibrium states (regardless of whether these are *globally* stable or only *metastable*).

We may rearrange Eqs. (2.11) and (2.12) to give

$$\rho_i=\frac{\lambda c_i}{1+\lambda c_i},\quad i=1,\ldots,\mathcal{N}, \tag{2.13}$$

and

$$\sum_i\frac{\lambda c_i}{1+\lambda c_i}-\mathcal{N}\bar{\rho}=0, \tag{2.14}$$

where

$$\lambda\equiv\exp(\beta\mu),$$

$$c_i\equiv\exp\left[-\beta\left(\Phi_i^{\mathrm{wf}}-\epsilon\sum_{j\neq i}^{\mathrm{NN}(i)}\rho_j\right)\right]. \tag{2.15}$$

We solve Eqs. (2.13) and (2.14) simultaneously for ρ_i and λ by iteration via

$$\rho_i^{(k+1)}=\frac{\lambda^{(k)}c_i^{(k)}}{1+\lambda^{(k)}c_i^{(k)}},\quad i=1,\ldots,\mathcal{N}, \tag{2.16}$$

and

$$\lambda^{(k+1)}=\lambda^{(k)}\left(\frac{\mathcal{N}\bar{\rho}}{\sum_i\rho_i^{(k+1)}}\right). \tag{2.17}$$

Convergence is assumed when $|(\mu^{(k+1)}-\mu^{(k)})/\mu^{(k)}|\leqslant 10^{-8}$.

C. Generation of fluid morphologies

In order to find the maximum number of solutions of the density distribution for a given value of $\bar{\rho}$, we solve the mean-field equations with different initial configurations. The first obvious choice is to fix all the local densities ρ_i's to the same value. For instance, starting from a low value of $\bar{\rho}$ and setting $\rho_i=\bar{\rho}$, we solve Eq. (2.13) using the algorithm described in the previous section. The converged density distribution corresponding to this value of $\bar{\rho}$ can then be used as a starting configuration for a new state at either higher or lower value of $\bar{\rho}$. However, this method does not ensure that we find all the solutions corresponding to the possible morphologies formed by the fluid over the surface, as we only generate solutions with a symmetry imposed by the ring pattern. In order to facilitate a search for solutions that "break" this symmetry we use the following method.

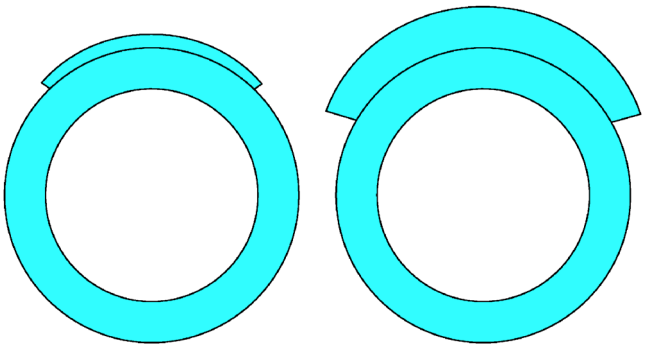

FIG. 2. (Color online) Illustration of the pattern extension used to generate asymmetric morphologies.

(1) We extend the pattern on one side of the ring (see Fig. 2). The lattice surface sites contained in this extended region interact with the fluid as a site contained into the ring pattern. The mean-field equations for this system are then solved in the *N-V-T* ensemble.

(2) The fluid density distribution generated from this surface geometry is used as a starting configuration for a system where only the original ring pattern is considered and we solve the mean-field equations in the *N-V-T* ensemble.

The size and position of the pattern extension can be modified (see Fig. 2), and this method allows us to find different classes of morphologies that may or may not present the axial symmetry imposed by the ring pattern. Depending on the pattern extension size, small variations of the Helmholtz free energy can be found within each class. We always consider the morphology with the lowest F.

III. RESULTS

A. Class of fluid morphologies formed over a ring-patterned surface

We first study the liquid morphologies formed over two rings of dimension 15-20 and 30-40, respectively. These two ring patterns have the same $R_{\mathrm{out}}/R_{\mathrm{in}}$ ratio but the length scale is larger for the second ring. The temperature is fixed at $T^*=kT/\epsilon=1.3$, corresponding to a ratio $T/T_c=0.86$ where T_c is the bulk critical temperature. The surface field is set to $\alpha=0.3$. The Helmholtz free energy of the fluid morphologies formed over the 15-20-ring-patterned surface is plotted as a function of the deviation of the total density from the bulk vapor coexistence density ($\Delta\rho=\bar{\rho}-\rho_v^b$) in Fig. 3. For the sake of clarity, the free energy of the bulk system, F_b, for the same overall density is subtracted from F. We clearly observe the existence of two branches in the free energy plot, intersecting at $\Delta\rho\simeq 0.0130$. These branches correspond to a ring and a spherical cap morphology presenting the axial symmetry of the underlying ring pattern. In Fig. 4 we represent snapshots of the ring and spherical cap. Only the "liquid" lattice sites—i.e., sites for which the local density fulfilled the criterion $\rho_i>0.5$—are represented [54]. The ring and spherical cap morphologies can either be stable, metastable, or unstable as a function of the total density of the system. Following the morphologies of the lowest Helmholtz free energy the liquid

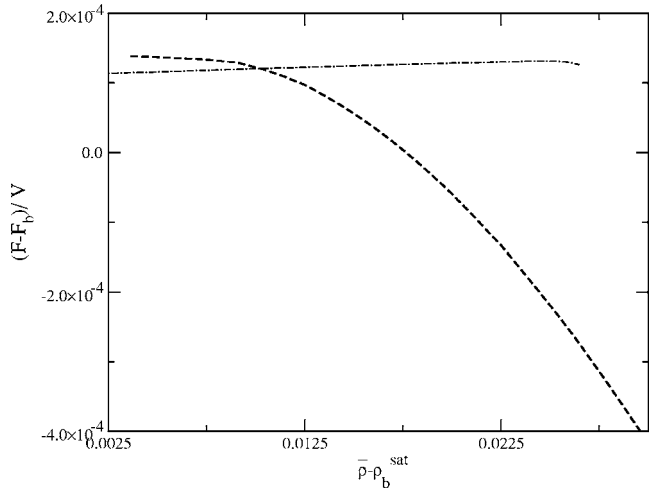

FIG. 3. Excess Helmholtz free energy per lattice site (in units of ϵ) for the 15-20-ring-patterned surface. Results are shown for the ring (dot-dashed lines) and spherical cap (dashed lines) morphologies. $T^*=1.3$, $\alpha=0.3$.

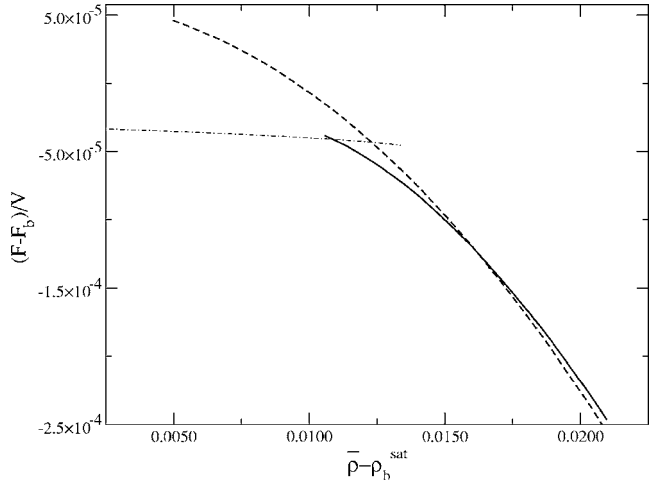

FIG. 5. Excess Helmholtz free energy per lattice site (in units of ϵ) for the 30-40-ring-patterned surface. Results are shown for the ring (dot-dashed lines), bulge (solid line) and spherical cap (dashed lines) morphologies. $T^*=1.3$, $\alpha=0.3$.

forms a covering over the ring at low density (or liquid volume). As the density increases, the number of layers over the pattern increases, thereby leading to a thickening of this ring morphology.

We mentioned earlier the difficult task of precisely defining a contact angle at a microscopic scale. For the droplets studied here the widths of the interfaces are not insignificant compared with the droplet size, so we use the equimolar dividing surface to locate the vapor-liquid interface. For the lattice gas model the dividing surface of the planar vapor-liquid interface occurs when the fluid density is equal to 0.5 and we assume that this is also true for the droplet. We make a linear fit of the position of the dividing surface for the first four layers of the droplet. The slope of this fit is simply related to the contact angle formed with the solid substrate. Even with this definition it can be difficult to precisely determine a contact angle especially for thin film morphologies like the ring.

When the system reaches densities $\Delta\rho > 0.0130$ the fluid takes a morphology where a cap of liquid forms over the ring and nonwetted region of the surface that it surrounds. At the contact line, the spherical cap interface is pinned by the pattern and the droplet forms a contact angle $\theta \simeq 110°$ with the surface. The contact angle increases with the volume of liquid in the cap due to the pinning of the vapor-liquid-solid contact line at the edges of the ring pattern.

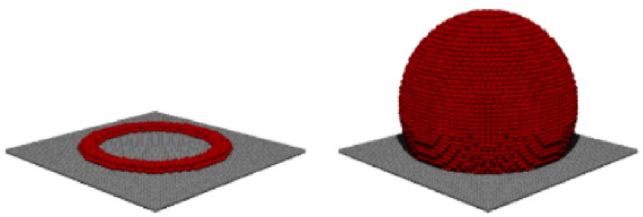

FIG. 4. (Color online) Snapshots of the classes of fluid morphologies formed over a 15-20-ring-patterned surface. Ring (left) and spherical cap (right) morphologies at $\Delta\rho=0.0130$. $T^*=1.3$, $\alpha=0.3$.

We now focus on the 30-40 ring. The Helmholtz free energy plot displays a third branch appearing at intermediate densities between the ring and the cap (Fig. 5). This branch intersects with the ring branch at $\Delta\rho \simeq 0.0110$ and with the cap branch at about $\Delta\rho \simeq 0.0162$. The liquid morphology corresponding to this new branch has a bulge shape which does not follow the symmetry of the underlying pattern. As can be seen in Figs. 6 and 7, the liquid forms regular layers over the whole ring pattern. However, at one side of the ring, a bulge of liquid is formed over the ring layers. This specific morphology can only be obtained by "breaking" the symmetry imposed by the ring pattern. The bulge morphology presents only a symmetry with respect to one plane normal to the surface and passing through the middle of the ring. The liquid formed over the substrate can now take three different morphologies: ring, bulge, and cap (see Fig. 6). As in the case of the 15-20 ring, the ring morphology is stable at low density and the liquid thickens over the ring pattern as $\bar{\rho}$ increases. Then a bulge is formed over a portion of the ring pattern. As the density increases, the bulge grows and progressively spreads over the nonwetting disc portion of the surface (see Fig. 8). The stability of this morphology reflects a balance between the interfacial tensions and the bulk free energy. We characterize the bulge morphology with two different contact angles θ_{in} and θ_{out}. These angles are defined in the plane of symmetry which bisects the ring and the bulge. Those two contact angles remain roughly constant at $\theta_{\text{out}} \simeq 120°$ and $\theta_{\text{in}} \simeq 180°$ as the bulge progressively covers over

FIG. 6. (Color online) Snapshots of the classes of fluid morphologies formed over a 30-40-ring-patterned surface. Ring (left) at $\Delta\rho=0.0104$, bulge (center) at $\Delta\rho=0.0144$, and spherical cap (right) at $\Delta\rho=0.0174$. $T^*=1.3$, $\alpha=0.3$.

FIG. 7. Lateral cut of the snapshots of the classes of fluid morphologies formed over a 30-40-ring-patterned surface. Ring (left) at $\Delta\rho=0.0104$, bulge (center) at $\Delta\rho=0.0144$, and spherical cap (right) at $\Delta\rho=0.0174$. $T^*=1.3$, $\alpha=0.3$.

the surface. When the liquid volume is large enough, a spherical cap is then formed and covers the whole area defined by the disc of radius R_{out}. Initially this cap has a contact angle of $\theta \simeq 90°$ with the surface, a value that as in the 15-20 case increases with the volume of liquid in the cap due to the pinning of the vapor-liquid-solid contact line at the edges of the ring pattern.

B. Influence of the ring dimension

We now investigate the influence of different parameters that may control the shape of the liquid morphologies formed over the patterned surface. We first consider the effect of a ring widening and the subsequent impact on the bulge morphology. In Fig. 9, we plot the Helmholtz free energy of the different liquid morphologies formed over a 30-50 ring. Similar to the 30-40 ring, we observe three different branches in this plot that we can associate with the ring, bulge, and cap morphologies. The bulge branch intersects with the ring branch at $\Delta\rho \simeq 0.0130$ and with the spherical cap at $\Delta\rho \simeq 0.0188$. The different morphologies are shifted to larger densities as compared to the 30-40 ring. An example of the bulge morphology is represented in Fig. 10. The overall shape of the bulge displays a smoother contour than the one found for the smaller ring, and the bulge is forming more of a bump geometry rather than a droplet on the ring. In other words the contact angle along the annulus is smaller for the 30-50 than for the 30-40 ring. The contact angles θ_{in} and θ_{out} formed by the bulge morphology with the surface in the symmetry plane are, however, very close to the 30-40 ring ones. The larger mean radius of curvature of the 30-50 ring allows us to accommodate more smoothly the fluid density variation along the annulus and the 30-50 bulge morphology is covering a larger area of the pattern than the 30-40 bulge. As the density increases, the system finally undergoes a morphological transition to a spherical cap forming a contact angle of $\theta \simeq 50°$ with the surface. This first stable cap morphology is forming a smaller contact angle with the surface than the 30-40 ring case. As the density increases, the cap volume increases with the vapor-liquid interface pinned at the outer rim of the pattern, therefore leading to an increasing of the observed contact angle.

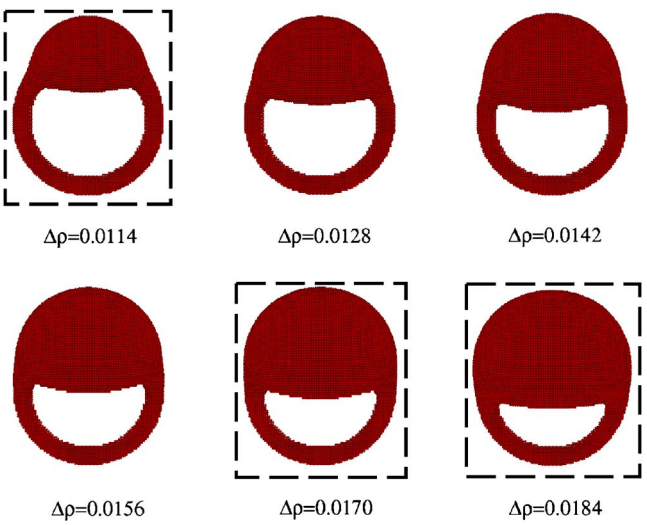

FIG. 8. (Color online) Bulge morphologies formed over a 30-40-ring-patterned surface as a function of the density. The dashed lines surrounding an image indicate metastable bulge morphologies with respect to the ring or the spherical cap. $T^*=1.3$, $\alpha=0.3$.

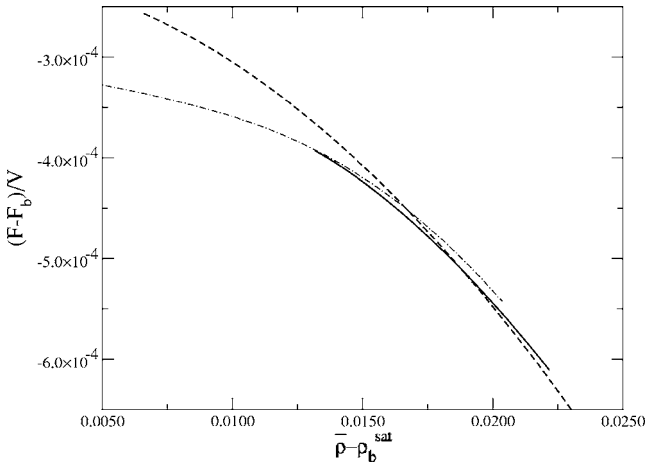

FIG. 9. Excess Helmholtz free energy per lattice site (in units of ϵ) for the 30-50-ring-patterned surface. Results are shown for the ring (dot-dashed lines), bulge (solid line), and spherical cap (dashed lines) morphologies. $T^*=1.3$, $\alpha=0.3$.

We may also note that the Helmholtz free energy of the bulge branch has a slope close to that for the ring and it becomes harder to observe a significant difference between the two. We can draw a parallel with the case of a homogeneous surface. If the wall-fluid interaction parameter α is weak enough, the fluid can form liquid droplets on top of the surface. As the interaction increases the contact angle of the droplets decreases, and finally when we reach the wetting transition (α_{wet}) the liquid can only organize into a film covering the whole surface area. When we increase the ring

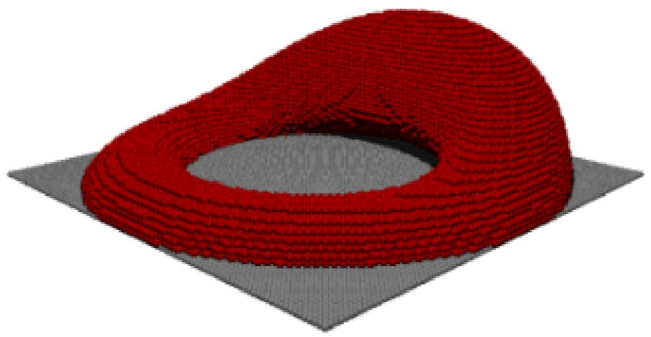

FIG. 10. (Color online) Bulge morphology over a 30-50-ring-patterned surface ($\Delta\rho=0.0158$). $T^*=1.3$, $\alpha=0.3$.

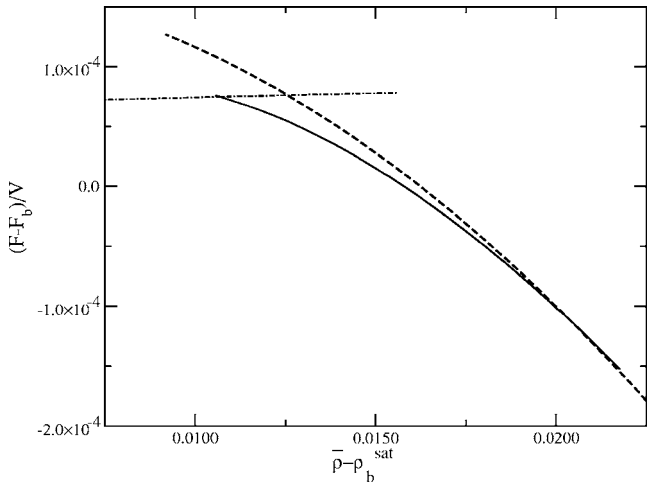

FIG. 11. Excess Helmholtz free energy for the 30-40-ring-patterned surface. Results are shown for the ring (dot-dashed lines), bulge (solid line), and spherical cap (dashed lines) morphologies. $T^*=1.3$, $\alpha=0.2$.

dimensions while maintening α constant at a value above α_{wet}, we increase the number of solid sites interacting with the liquid, and therefore this is equivalent to increasing the wall-fluid interaction parameter for a homogeneous surface. We observe that the bulge contact angle along the annulus is decreased compared to the case of the 30-40 ring. If the attractive surface area (i.e., the ring width) is large enough, the bulge will cease to be stable.

C. Influence of the surface field

We now focus on the effect of the field strength imposed by the ring pattern and modify the wall-fluid interaction parameter α. We consider a 30-40 ring where we set $\alpha=0.2$. We now fall into a regime of partial wetting of the ring pattern, even though a uniform surface with the same value of α would be completely wetted by the liquid. Indeed, for low $\bar{\rho}$, the stable branch of the Helmholtz free energy (Fig. 11) corresponds to a low-density ring forming over the pattern where the corresponding local densities $\rho_i<0.5$. The density is insufficient to form a liquid film over the pattern, and as a consequence, the ring appears *dry*. As the density increases, the system undergoes a morphological transition to a bulge state at $\Delta\rho\simeq0.0107$. In Fig. 12, we plot a sequence of snapshots corresponding to the evolution of the bulge morphology as the density increases. We observe that a liquid droplet develops on one side of the ring pattern. Rather than forming a thin film over the whole pattern, the system prefers to accommodate a partial wetting situation where a droplet is forming over a partial area of the pattern. As the density increases, the bulge spreads over the nonwetting disk inside the pattern but is always partially wetting the ring. When $\Delta\rho=0.0206$, the bulge branch crosses the cap branch and a spherical cap is formed over the ring and nonwetted region of the surface that it surrounds. The contact angle formed by this cap with the surface is $\theta\simeq90°$. Again, due to pinning of the three-phase contact line at the ring edge, the contact angle increases with the volume of the cap.

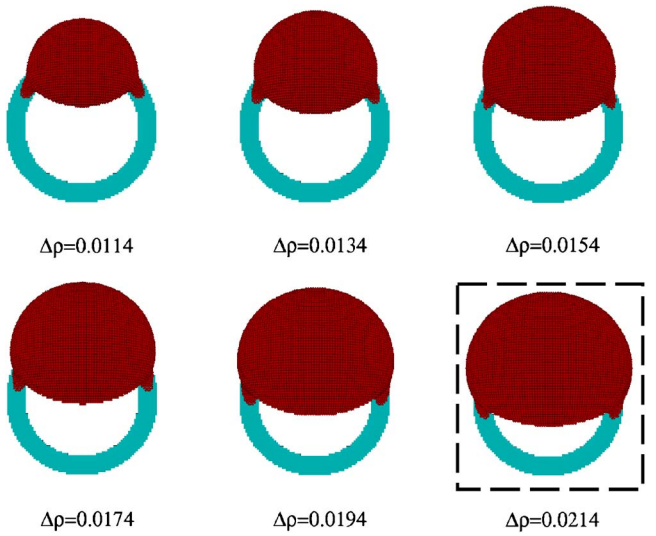

FIG. 12. (Color online) Bulge morphologies formed over a 30-40-ring-patterned surface as a function of the density. The dashed lines surrounding an image indicate metastable bulge morphologies with respect to the spherical cap. $T^*=1.3$, $\alpha=0.2$.

D. Influence of the temperature

Finally in order to make a closer connection with the way experiments are conducted, we perform a set of calculations in which we change the temperature of the system while the total density is kept constant. We initialize the system to a bulge morphology found in a 30-40 ring system with $\alpha=0.3$. The different morphologies obtained as a function of the temperature are shown in Fig. 13. As we expect, the cooling of the system leads to an increased covering of the nonwetting disk by the bulge and finally to the formation of a spherical cap. On the other hand, when the temperature increases, the bulge volume decreases until a temperature where a ring covers the pattern. Therefore, the same morphologies are found if we change either the temperature or the average density.

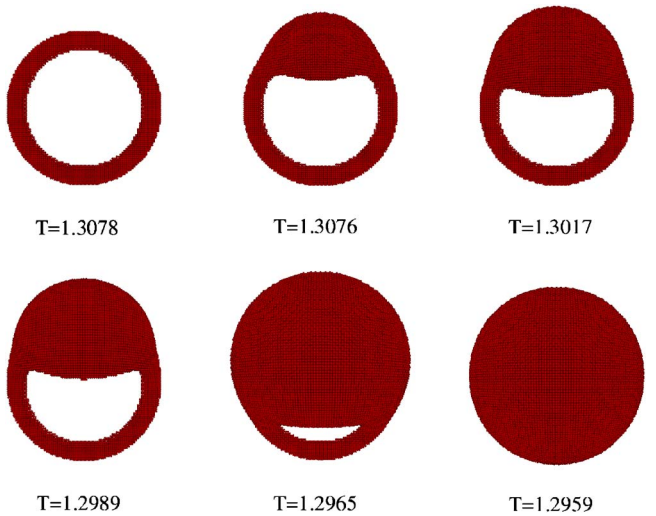

FIG. 13. (Color online) Bulge morphologies formed over a 30-40-ring-patterned surface as a function of the temperature. $\Delta\rho=0.0138$, $\alpha=0.3$.

IV. CONCLUSIONS

We have investigated the behavior of fluid wetting substrates decorated with nanometric ring patterns by performing calculations at a molecular level using MF-DFT for a lattice model. The formation of droplets on surfaces corresponds to a region of bulk vapor metastability where the bulk liquid is stable. The grand canonical ensemble is therefore unsuited to study this problem since the variations of the total density would preempt the morphological transitions related to the droplet. We therefore implement an algorithm where the total density of the system is fixed.

The calculations show that a liquid adsorbed on a ring nanopatterned surface can exhibit three classes of morphologies as a function of the volume of liquid. At low density, the fluid is structured into layers above the ring pattern. This morphology thickens as the density increases until the liquid undergoes a morphological transition to a bulge where a droplet of liquid forms on one side of the ring. The density is no longer homogeneous along the annulus, and the liquid morphology does not present the axial symmetry imposed by the ring geometry. The existence of this transition is, however, subject to a minimum length scale necessary to form the bulge morphology and to a maximum ring width beyond which the bulge ceases to exist. The balance between the interfacial tensions and the bulk free energy governs these conditions. As the density increases, the system undergoes another morphological transition to a spherical cap that covers the disk of radius R_{out}. When the ring dimension increases, the first stable cap covering the pattern is formed with a lower contact angle. As the density increases, the contact angle increases. The cap morphologies found in our calculations are pinned to the interface by the ring boundary. This is probably because the *reference* surface does not interact with the fluid as we set the wall-fluid potential to zero for any surface sites that do not belong to the pattern. Therefore, this surface is totally nonwetting for the fluid. If we tuned the interaction of the *reference* surface to decrease the contrast between the pattern and the remainder of the surface, the pinning condition should disappear and the cap would spread outside the pattern interface.

An interesting behavior occurs when we decrease the surface field. The weakening of the field leads to a situation of partial wetting where, at low density, no liquid is homogeneously adsorbed over the pattern and therefore the ring pattern is essentially dry even though a uniform surface with the same value of α would be completely wetted by the liquid. The first liquid state found is a bulge that wets a part of the ring while the remainder of the pattern is dry. In future work it would be interesting to investigate the nature of the transition between the wetting and partial wetting states and its dependence upon the ring geometry.

FIG. 14. (Color online) Bulge morphology obtained in *N-V-T* Monte Carlo simulations for a 30-40-ring-patterned surface. $T/T_c = 0.86$, $\alpha = 0.3$.

In experiments, the different liquid morphologies are obtained by changing the temperature of the system that consequently leads to a change of the liquid volume [14]. If we perform calculations by cooling down or heating up the system, we also found the same behavior as the one found by modifying the density at constant temperature. The behavior found in this work is in very good agreement with experiments and calculations performed at a micrometer scale [14,28]. Beyond that, this work demonstrates the suitability of the lattice model to study wetting of nanopatterned surfaces. The behavior seen in our MF-DFT calculations is also observed in Monte Carlo simulations. As an illustration, we plot in Fig. 14 a preliminary result from a Monte Carlo simulation in the *N-V-T* ensemble obtained at the same ratio T/T_c for the 30-40 ring and $\alpha = 0.3$. The same bulge morphology seen in the MF-DFT calculations is obtained. It is perhaps worthwhile to point out that the number of particles in this simulation is $N \simeq 0.5 \times 10^6$. A comparable calculation with an off-lattice model would be very expensive indeed.

ACKNOWLEDGMENTS

Research on this project at the University of Massachusetts was supported by a grant from the National Science Foundation (No. CTS-0220835). Two of us (P.A.M. and M.S.) also acknowledge financial support from the Sonderforschungsbereich 448 "Mesoskopisch strukturierte Verbundsysteme" which made possible in part the sabbatical visit of P.A.M. at the Technische Universität Berlin during which this work was initiated.

[1] S. Ono and S. Kondo, in *Encyclopedia of Physics*, edited by S. Flugge (Springer, Berlin, 1960), Vol. 10.
[2] J. Rowlinson and B. Widom, *Molecular Theory of Capillarity* (Clarendon, Oxford, 1982).
[3] D. Bonn and D. Ross, Rep. Prog. Phys. **64**, 1085 (2001).
[4] T. Young, Philos. Trans. R. Soc. London **95**, 65 (1805).
[5] R. D. Gretz, J. Chem. Phys. **45**, 3160 (1966).
[6] A. B. D. Cassie and S. Baxter, Trans. Faraday Soc. **40**, 546 (1944).
[7] A. B. D. Cassie, Discuss. Faraday Soc. **3**, 11 (1948).

[8] R. N. Wenzel, Ind. Eng. Chem. **28**,. 988 (1936).
[9] D. W. L. Tolfree, Rep. Prog. Phys. **61**, 313 (1998).
[10] F. Burmeister, C. Schäfle, B. Keilhofer, C. Bechinger, J. Boneberg, and J. Leiderer, Adv. Mater. (Weinheim, Ger.) **10**, 495 (1998).
[11] A. Kumar and G. M. Whitesides, Appl. Phys. Lett. **63**, 2002 (1993).
[12] P. Zeppenfeld, V. Diercks, R. David, F. Picaud, C. Ramseyer, and C. Girardet, Phys. Rev. B **66**, 085414 (2002).
[13] C. Schäfle, C. Bechinger, B. Rinn, C. David, and P. Leiderer, Phys. Rev. Lett. **83**, 5302 (1999).
[14] C. Schäfle, Ph.D. Thesis, University of Konstanz, Konstanz, Germany, 2002.
[15] P. Lenz, C. Bechinger, C. Schäfle, P. Leiderer, and R. Lipowsky, Langmuir **17**, 7814 (2001).
[16] S. Harkema, E. Schäffer, M. D. Morariu, and U. Steiner, Langmuir **19**, 9714 (2003).
[17] D. Öner and T. J. McCarthy, Langmuir **16**, 7777 (2000).
[18] M. Schoen and D. J. Diestler, Phys. Rev. E **56**, 4427 (1997).
[19] H. Bock and M. Schoen, Phys. Rev. E **59**, 4122 (1999).
[20] H. Bock, D. J. Diestler, and M. Schoen, J. Phys.: Condens. Matter **13**, 4967 (2001).
[21] M. H. Adão, M. de Ruijter, M. Voué, and J. De Coninck, Phys. Rev. E **59**, 746 (1999).
[22] L. J. D. Frink and A. G. Salinger, J. Chem. Phys. **110**, 5969 (1999).
[23] C. Bauer and S. Dietrich, Phys. Rev. E **60**, 6919 (1999).
[24] M. Schneemilch and N. Quirke, Mol. Simul. **29**, 685 (2003).
[25] M. Schneemilch, N. Quirke, and J. R. Henderson, J. Chem. Phys. **118**, 816 (2003).
[26] A. Dupuis and J. M. Yeomans, FGCS, Future Gener. Comput. Syst. **20**, 993 (2004).
[27] N. Pesheva and J. De Coninck, Phys. Rev. E **70**, 046102 (2004).
[28] P. Lenz and R. Lipowsky, Phys. Rev. Lett. **80**, 1920 (1998).
[29] H. Gau, S. Herminghaus, P. Lenz, and R. Lipowsky, Science **283**, 46 (1999).
[30] R. Lipowsky, P. Lenz, and P. S. Swain, Colloids Surf., A **161**, 3 (2000).
[31] R. Lipowsky, Interface Sci. **9**, 105 (2001).
[32] R. Lipowsky, Curr. Opin. Colloid Interface Sci. **6**, 40 (2001).
[33] M. Brinkmann and R. Lipowsky, J. Appl. Phys. **92**, 4296 (2002).
[34] G. Chmiel, A. Patrykiejew, W. Rzysko, and S. Sokolowksi, Mol. Phys. **83**, 19 (1994).
[35] C. Rascon and A. O. Parry, J. Chem. Phys. **115**, 5258 (2001).
[36] P. Lenz, W. Fenzl, and R. Lipowsky, Europhys. Lett. **53**, 618 (2001).
[37] R. Lipowsky, M. Brinkmann, R. Dimova, T. Franke, J. Kierfeld, and X. Z. Zhang, J. Phys.: Condens. Matter **17**, 537 (2005).
[38] R. Seemann, M. Brinkmann, E. J. Kramer, F. F. Lange, and R. Lipowsky, Proc. Natl. Acad. Sci. U.S.A. **102**, 1848 (2005).
[39] M. Brinkmann, J. Kierfeld, and R. Lipowsky, J. Phys. A **37**, 11547 (2004).
[40] A. Valencia and R. Lipowsky, Langmuir **20**, 1986 (2004).
[41] E. Kierlik, P. A. Monson, M. L. Rosinberg, L. Sarkisov, and G. Tarjus, Phys. Rev. Lett. **87**, 055701 (2001).
[42] E. Kierlik, P. A. Monson, M. L. Rosinberg, and G. Tarjus, J. Phys.: Condens. Matter **14**, 9295 (2002).
[43] H. J. Woo and P. A. Monson, Phys. Rev. E **67**, 041207 (2003).
[44] F. Detcheverry, E. Kierlik, M. L. Rosinberg, and G. Tarjus, Langmuir **20**, 8006 (2004).
[45] F. Porcheron, P. A. Monson, and M. Thommes, Langmuir **20**, 6482 (2004).
[46] F. Porcheron, P. A. Monson, and M. Thommes, Adsorption **11**, 325 (2005).
[47] L. Sarkisov and P. A. Monson, Phys. Rev. E **65**, 011202 (2001).
[48] H. T. Davis, *Statistical Mechanics of Phases, Interfaces, and Thin Films* (Wiley-VCH, New York, 1996).
[49] K. Binder, Physica A **319**, 99 (2003).
[50] L. G. MacDowell, P. Virnau, M. Muller, and K. Binder, J. Chem. Phys. **120**, 5293 (2004).
[51] G. L. Aranovich and M. D. Donohue, Phys. Rev. E **60**, 5552 (1999).
[52] A. V. Neimark and P. I. Ravikovitch, Stud. Surf. Sci. Catal. **128**, 51 (2000).
[53] J. Sommerfeld, H. Bock, and M. Schoen, in Statistical Physics and Beyond: Second Mexican Meeting of Statistical and Experimental Physics, edited by F. J. Uribe, L. Garcia-Colin, and E. Diaz-Herrera, AIP Conf. Proc. (AIP, Melville, NY, 2005), p. 37.
[54] A. Valencia, M. Brinkmann, and R. Lipowsky, Langmuir **17**, 3390 (2001).